A Modified Pre-Fluxing Method for the Energization of Single-Phase Transformers

A. Aghazadeh, K. Li, *Senior Member, IEEE*, M. Popov, *Fellow, IEEE,* V. Terzija, *Fellow, IEEE,*
and S. Azizi, *Senior Member, IEEE*

Abstract—Inrush current refers to the high-magnitude excitation current drawn by a transformer upon energization. The intensity of inrush current is a function of the residual flux of the transformer's core and the voltage magnitude at the energization instant. This paper proposes a method to effectively mitigate the inrush current of single-phase transformers. The proposed method overcomes the shortcomings of the well-established pre-fluxing method, and thus, is referred to as the modified pre-fluxing method. The method operates without requiring any prior knowledge regarding the transformer's design information or parameters. Accounting for uncertainties in circuit breaker closing operation, the core's residual flux is modified to an appropriate reference value, minimizing the corresponding adverse impact. The flux adjustment is accomplished by a power electronic circuitry that applies suitable voltage across the transformer's low-voltage winding. The core's residual flux is estimated after removing the DC offset present in the measured open-circuit voltage. The energization process is then initiated at an appropriate instant ensuring the core's steady-state flux matches its adjusted residual flux. The efficiency of the modified pre-fluxing method is demonstrated by conducting 12,000 simulations in PSCAD/EMTDC. A hardware-in-the-loop (HIL) setup composed of a transformer and pre-fluxing device is used for extensive experimental validation and comparison with recent energization methods under more realistic conditions.

Index Terms— Inrush current, pre-fluxing method, residual flux, single-phase transformer, transformer energization.

I. INTRODUCTION

SINGLE-PHASE power transformers play a vital role in different applications within transmission and distribution systems, along with railway feeding systems. Electrically coupled single-phase transformers can form a three-phase transformer bank which may be preferred over a conventional three-phase transformer, particularly in extra high-power applications. This preference is driven by the potential for increased reliability, flexibility, simplified transportation, better load distribution, and easier maintenance [1].

Energizing a transformer can result in temporary flow of high-magnitude excitation current referred to as inrush current [2]. This current is attributed to the nonlinearity of the transformer core and its memory-dependent magnetic properties, requiring several cycles to settle down the steady-

Amir Aghazadeh, Kang Li, and Sadegh Azizi are with the School of Electronic and Electrical Engineering, University of Leeds, Leeds LS2 9JT, UK (e-mail: elaagh@leeds.ac.uk; k.li1@leeds.ac.uk; s.azizi@leeds.ac.uk).

Marjan Popov is with the Faculty of Electrical Engineering, Mathematics and Computer Science, Delft University of Technology, Delft 2628CD, the Netherlands (e-mail: m.popov@tudelft.nl).

Vladimir Terzija is with the School of Engineering, Newcastle University, Newcastle NE1 7RU, UK (e-mail: vladimir.terzija@newcastle.ac.uk).
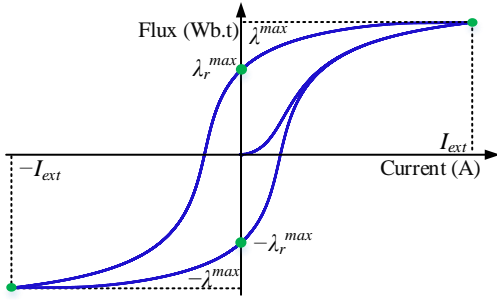
state excitation current [3]. This would subject the transformer windings to excessive axial and radial forces [2], [4]. Inrush current is rich in DC and harmonic components, which can trouble protective relays, prolong the energization process, and lead to power quality issues such as voltage sags, harmonic distortions, and transient overvoltages.

Several methods have been proposed thus far to address the challenges faced by protective relays during transformer energization [5-7]. These methods, in principle, aim to differentiate between inrush and fault currents. This can potentially address the malfunction issues of protective relays but leaves the transformer to unnecessarily endure inrush current, thus reducing the transformer's lifetime [8]. Methods designed to mitigate inrush current can simultaneously overcome protection system issues and reduced transformer lifetime. A trivial technique to accomplish this aim is to temporarily increase the circuit's resistance using a series resistor [9, 10] or a power electronics-based current limiter [11-13]. The authors in [14] propose an energization technique that gradually increases the voltage applied to the transformer using a power electronics-based device. The methods proposed in [9-14] require complicated design modifications and/or control mechanisms, leading to augmented manufacturing and maintenance costs.

The mismatch between residual and prospective fluxes is the main reason that a transformer draws inrush current upon energization. In this context, residual flux refers to the magnetic field that remains trapped inside the transformer core due to the hysteresis phenomenon following de-energization [15]. Prospective flux represents the anticipated flux at the energization instant, assuming the transformer had already attained a steady state [16]. References [17], [18], and [19] propose methods for matching the residual and prospective fluxes by controlling the closing operation of circuit breakers (CBs). The success of these methods is highly dependent on the accurate knowledge of residual flux at the instant of transformer de-energization [20, 21]. More importantly, the performance of these methods can be compromised by changes in the residual flux of the de-energized transformer due to a phenomenon known as ringdown transient [22].

To overcome the limitations of methods that rely on prior knowledge of residual flux, references [23, 24] propose a demagnetization method to effectively neutralize the core's residual flux using a DC voltage source. The transformer is then energized at the voltage peak to match the residual and prospective fluxes, thus eliminating inrush current. In practice, however, the residual flux cannot be entirely removed by the demagnetization method. More importantly, aiming for the

Fig. 1. Major hysteresis loop during transformer nominal operation.

Fig. 2. Pre-fluxing devices used for flux adjustment.

voltage peak during transformer energization is not advisable as it amplifies the impact of uncertainties associated with the circuit breaker closing operation. As a compromise solution, the target point on the voltage waveform can be intentionally shifted to a point slightly preceding the peak for energization [25]. The challenge in matching the residual and prospective fluxes is a significant drawback of the demagnetization method, which limits its ability to completely eliminate inrush current.

References [26-28] propose a method called "pre-fluxing" to adjust the residual flux to either of two predetermined values using a pre-fluxing device. The time this method needs for flux adjustment increases significantly as the transformer power rating increases. The requirement to adjust the residual flux to only two specific values makes it challenging or even impossible to match the residual and prospective fluxes. Indeed, the operating characteristics of CBs may prevent attaining certain prospective fluxes. To overcome the foregoing drawback, an effective flux matching method is suggested in [29] that provides greater flexibility in flux adjustment. However, this method would still need to know the size of the peak excitation current, which usually is not available on transformers' nameplates.

This paper proposes a *pre-fluxing method* to mitigate the inrush current of single-phase power transformers. This method offers the advantage of not requiring detailed information about the transformer design, as it relies solely on measurements for flux adjustment. The proposed method is very fast regardless of the transformer size and can adjust its residual flux to any desired value within the feasible range. Rigorous flux estimation (and thus adjustment) is made possible by compensating the DC offset normally present in voltage and current measurements provided by commercial transducers. Extensive simulations carried out in PSCAD/EMTDC, along with comprehensive experiments conducted on a hardware-in-the-loop (HIL) test system, validate the method's effectiveness in mitigating inrush current. Obtained results confirm the superiority of the proposed method over the demagnetization [25] and conventional pre-fluxing [28] methods in different conditions.

II. PRE-FLUXING: THEORETICAL FRAMEWORK AND CHALLENGES

Let λ and i_{ext} denote the magnetic flux within the transformer's core and the excitation current flowing into the transformer, respectively. The value of λ at any given time is not only determined by the magnitude of i_{ext} but also by its rate
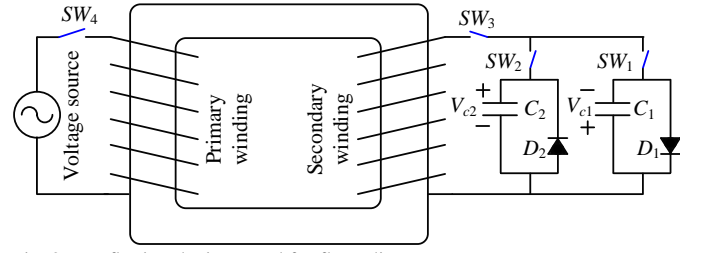
of change. This is a nonlinear relationship characterized by hysteresis curves. The hysteresis curve shown in Fig. 1 represents the major hysteresis loop traversed during the steady-state operation of the transformer. Throughout this cycle, the flux and current vary between the positive and negative maximum fluxes ($\pm\lambda^{max}$) and positive and negative peak excitation currents ($\pm I_{ext}$), respectively. The maximum feasible residual fluxes ($\pm\lambda_r^{max}$) represent the highest value to which the flux can settle once the transformer is de-energized.

To explain why a transformer draws inrush current, let us consider the scenario where the nominal voltage $v(t) = V_m cos(\omega t)$ is applied to the primary winding of an unloaded single-phase transformer, at $t = t_0$. Utilizing Faraday's law, the core's flux can be calculated from

$$\lambda(t) = \int_{t_0}^{t} V_m \cos(\omega t)\, dt + \lambda_r$$

$$= \underbrace{\lambda^{max}\sin(\omega t)}_{Steady-state\ component} \underbrace{-\overbrace{\lambda^{max}\sin(\omega t_0) + \lambda_r}^{\lambda_p}}_{DC\ component} \quad (1)$$

where, $\lambda^{max} = V_m/\omega$ signifies the maximum flux in the nominal operating condition, and λ_r and λ_p represent residual and prospective fluxes. As per (1), the flux would be sinusoidal immediately after energization only if $\lambda_p = \lambda_r$. Otherwise, a DC offset would be present in the flux waveform, which could drive the transformer core into saturation. This saturation causes significant fluctuations in i_{ext} with minor variations of λ, which will be seen as high-magnitude inrush current [29].

The pre-fluxing method proposed in [28] adjusts the residual flux from any unknown value in the feasible range [$-\lambda_r^{max}, \lambda_r^{max}$] to λ_r^{max}. To differentiate the initial value of residual flux λ_r from the adjusted value, let us denote the core's adjusted residual flux (through the flux adjustment process) as λ_r^{ad}. The core's flux is adjusted by a device shown in Fig. 2, comprising two charged capacitors (C_1 and C_2), two antiparallel diodes (D_1 and D_2), and three switches (SW_1 to SW_3). This device initiates the flux adjustment procedure by connecting C_1 to the transformer via SW_1. Once C_1 is fully discharged, D_1 bypasses the capacitor. When the current through D_1 reaches zero, both C_1 and D_1 are disconnected by SW_1. This process is repeated with C_2. Ultimately, the residual flux is adjusted to λ_r^{max}, and the pre-fluxing device is disconnected by SW_3. The flux adjustment is followed by energizing the transformer by SW_4 at an appropriate voltage angle to match the residual and prospective fluxes (i.e., $\lambda_p = \lambda_r^{ad}$).

Let us consider a scenario where C_1 has just been bypassed by D_1, and the current of D_1 is at its peak value. In this condition, the transformer can be represented by an equivalent
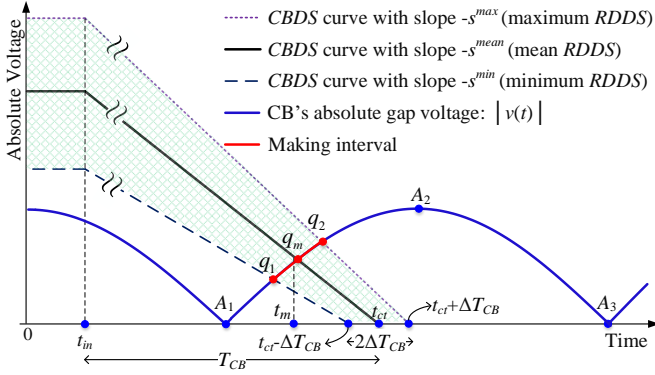
Fig. 3. Impact of scatter on the making instant.

Fig. 4. Preferred making range and corresponding safe flux range.

inductor (L_{eq}) and a resistor (R_{eq}), forming an RL circuit without a voltage source. The time constant of the zero response of this first-order circuit is $\tau = L_{eq}/R_{eq}$ [30]. Practically speaking, it takes 5τ for the current to descends to zero. Since $L_{eq} \gg R_{eq}$ for high-power transformers, a substantial amount of time is required for the current to decay. This means with an increase in the power rating of the transformer, the time needed for flux adjustment by the pre-fluxing method significantly increases. It follows that the pre-fluxing method is quite slow for high-power transformers. Another major challenge the conventional pre-fluxing method faces is the difficulty of ensuring the transformer is switched on such that $\lambda_p - \lambda_r^{ad}$ is minimized. This results from the operating characteristics/limitations of CBs. In practice, these limitations often make it challenging, if not impossible, to energize the transformer at the required instant. Therefore, the pre-fluxing method proposed in [28] struggles to achieve its full potential in realistic conditions.

III. SAFE FLUX RANGE ASSOCIATED WITH CB CLOSING OPERATION

Fig. 3 shows a typical CB dielectric strength (*CBDS*) curve, associated with the closing operation of a CB while the nominal voltage $v(t) = V_m cos(\omega t)$ is applied to the transformer. The operation begins at $t = t_{in}$ and continues until a metal-to-metal contact is made between the fixed and moving poles of the CB at the contact touch instant t_{ct}. The time difference between t_{in} and t_{ct} is referred to as closing time (T_{CB}). As the moving contact approaches the fixed contact, the *CBDS* decreases at the rate of decrease of dielectric strength (*RDDS*) [31]. The *CBDS* curve intersects the CB gap voltage (the voltage across the CB poles) at the making instant t_m. Due to establishment of an arc, the instant when the CB begins to conduct electricity (known as making instant) occurs before physical contact is made at $t = t_{ct}$ [32]. The making instant corresponding to a given t_{ct} is the smallest t that satisfies the following equation:

$$|v(t)| + s(t - t_{ct}) = 0 \qquad (2)$$

where $v(t)$ is the CB's instantaneous gap voltage and s shows the value of *RDDS*.

In practical applications, the closing operation of CBs involves uncertainties that affect both the *RDDS* and the closing time of the CB, causing variations at each energization attempt [17], [33]. The uncertainty associated with *RDDS* is referred to
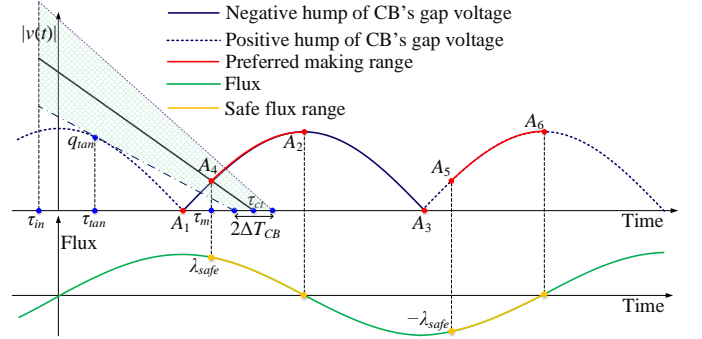
as *RDDS* scatter, which results in *RDDS* variation within the range $[s^{min}, s^{max}]$, with expected value s^{mean}. Similarly, mechanical scatter, shown by ΔT_{CB}, represents the uncertainty related to the closing time of the CB. The closing time spreads over a range with length $2\Delta T_{CB}$ and mean T_{CB}, making the contact touch instant fall within the range $[t_{ct} - \Delta T_{CB}, t_{ct} + \Delta T_{CB}]$. Therefore, the *CBDS* in most of cases does not coincide with the solid black line in Fig. 3, which demonstrates the scenario with no scatter (i.e., meaning *RDDS*= s^{mean} and $t_{ct} = t_{in} + T_{CB}$). Instead, the *CBDS* curve would slightly vary in different closing attempts, while remaining within the shaded quadrilateral region shown in Fig. 3. This variation results in a true making instant slightly different from t_m.

The making point does not necessarily fall on q_m but somewhere in the making interval. This interval, shown in red in Fig. 3, spans from q_1 to q_2 on the absolute gap voltage. The deviation from the ideal target making instant would be smaller if the transformer gets energized anywhere from A_1 to A_2 rather than from A_2 to A_3. This is why it is recommended to energize the transformer only on the rising half of an absolute gap voltage hump [34]. Following this recommendation reduces the impact of *RDDS* and mechanical scatter (i.e., makes the making interval smaller). It is also advisable to initiate the energization process closer to the lower end of the range from A_1 to A_2 since points closer to A_1 exhibit even less sensitivity to scatter [34].

Makings that occur overly close to A_1 would cause the shaded quadrilateral region of Fig. 3 to expand significantly. In such a condition, the region's lower side could intersect with the previous hump, which would lead to a huge difference between λ_r^{ad} and λ_p. To avoid this, the closing operation must commence after a certain instant called the critical initiation instant, hereafter. This instant marks the earliest instant ensuring no risk of making on the previous hump, even under extreme conditions. To obtain the critical initiation instant, the quadrilateral region shown in Fig. 3 must be left-shifted until its lower side becomes tangent to the previous hump at q_{tan}, as shown in Fig. 4. To distinguish between the time instants in Fig. 3 and those in Fig. 4, in the latter the letter t is replaced by the Greek letter τ. The lower side of the quadrilateral region of Fig. 4 is associated with $\tau_{ct} - \Delta T_{CB}$ and s^{min}. Thus, the absolute gap voltage derivative at τ_{tan} equals $-s^{min}$, as follows:

$$-\omega V_m \sin(\omega \tau_{tan}) = -s^{min} \qquad (3)$$

Hence, $\tau_{tan} = \sin^{-1}\left(\frac{s^{min}}{\omega V_m}\right)\Big/\omega$. The critical contact touch
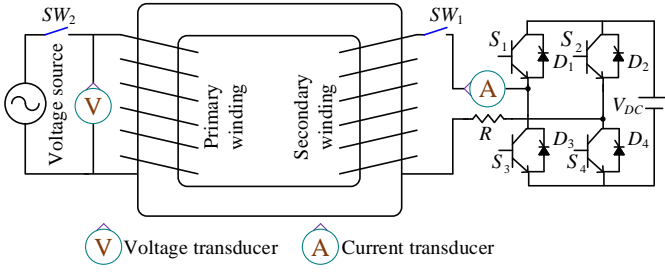
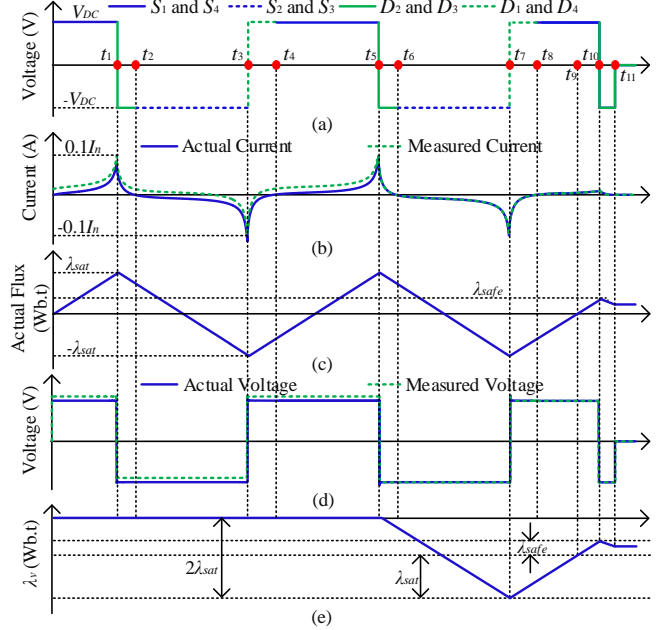Fig. 5. Pre-fluxing device used by the proposed method.

Fig. 6. (a) Secondary winding voltage, (b) actual and measured currents, (c) actual flux, (d) primary winding actual and measured voltage, and (e) voltage integral.

instant (τ_{ct}) is obtained from

$$|V_m \cos(\omega\tau_{tan})| = s^{min}((\tau_{ct} - \Delta T_{CB}) - \tau_{tan}) \quad (4)$$

One can then obtain τ_{ct} as:

$$\tau_{ct} = \tau_{tan} + \Delta T_{CB} + \frac{|V_m \cos(\omega\tau_{tan})|}{s^{min}} \quad (5)$$

Initiating the closing operation after $\tau_{in} = \tau_{ct} - T_{CB}$ would effectively prevent from making on the previous hump. Now, the maximum prospective flux achievable by a CB (without the risk of making on the previous hump) needs to be calculated. To this end, the making instant (τ_m) associated to τ_{ct} and s^{mean} are obtained. This instant, linked to the making at A_4 in Fig. 4, is calculated by substituting τ_{ct} and s^{mean} into (1). Point A_4 shows the lower limit of the preferred making range that spans from A_4 to A_2. On the next hump, this range spans from A_5 to A_6 on the rising half of the positive gap voltage. The flux corresponding to A_4 is denoted by λ_{safe} and obtained from

$$\lambda_{safe} = \lambda^{max} \sin(\omega\tau_m) \quad (6)$$

Choosing the rising half of the positive gap voltage sets the lower limit of this range at $-\lambda_{safe}$, which corresponds to A_5 as target making instant. Combining these two pieces yields the range $[-\lambda_{safe}, \lambda_{safe}]$ which is referred to as the safe flux range. Any value in the safe range is the prospective flux of a target making instant that involves no risk of making on the previous hump. Flux values closer to the lower and upper bounds of the safe range (which respectively corresponds to A_4 and A_5) are preferred since they are associated with less sensitivity to *RDDS* and mechanical scatter. Depending on the core material, λ_r^{max} may or may not fall in the safe range. In the case of the latter, inrush current cannot be dealt with properly using the pre-fluxing method [28]. This is because the transformer might get energized undesirably within the previous hump, thereby rendering high-magnitude inrush current unavoidable.

IV. PROPOSED MODIFIED PRE-FLUXING METHOD

This section explains the modified pre-fluxing method proposed for energizing single-phase transformers. Hereafter, the proposed method is referred to as MPFM, and the conventional method of [29] is referred to as CPFM. The modifications made in MPFM are necessary to accelerate the energization process for high-power transformers. To further improve the performance, MPFM is designed such that it can adjust the residual flux to any value within the feasible range [−λ_r^{max}, λ_r^{max}]. This adjustment aims to strike a balance between two conflicting factors: Minimizing the impact of CB scatter

while ensuring no risk of making on the previous hump. After flux adjustment, the transformer is energized at an instant that minimizes the difference between λ_r^{ad} and λ_p.

A. Pre-fluxing Device

For flux adjustment, MPFM employs a pre-fluxing device shown in Fig. 5. This device is composed of a full-bridge single-phase inverter (with four switches S_1-S_4 and four anti-parallel diodes D_1-D_4), a DC voltage source with voltage denoted as V_{DC}, and a resistor connected in series with the transformer. A voltage transducer and a current transducer are employed to measure the voltage induced on the open-circuited primary winding and the current injected into the transformer by the pre-fluxing device. The theory behind determining the voltage of the DC voltage source is explained in [23]. The resistor ensures that the current of the pre-fluxing device does not exceed the peak value of the transformer's nominal current. The size of the resistor can be readily determined from $R = V_{DC}/I_n$, where I_n is the transformer's nominal peak current.

B. Residual Flux Adjustment Stage

A method is proposed in this subsection for adjusting the residual flux from an initial unknown value of λ_r to values that can be met by the prospective flux, given the limitations of the CB. This is achieved by applying a square-wave voltage to the transformer via the pre-fluxing device and regulating the current flowing into the transformer. For new transformers employing highly efficient designs, the excitation current ranges from 0.1% to 1% of the nominal transformer current, while this value can increase to as high as 6% for older transformers [35]. This means that when the excitation current reaches $0.1I_n$ at $t = t_1$, it is guaranteed that the transformer has been driven into saturation.

For the sake of illustration, let us assume that the pre-fluxing device is connected to the secondary winding of the transformer

with an initial residual flux of $\lambda_r = 0$ (without loss of generality). To start the flux adjustment, switches S_1 and S_4 are turned on at $t = 0$, and positive voltage (V_{DC}) is applied to the transformer, as shown in Fig. 6(a). Fig. 6(b) demonstrates the waveforms of the actual and measured currents during flux adjustment. Current flows through switches S_1 and S_4. At $t = t_1$, the measured current reaches $0.1I_n$. The actual current is different from the measured current due to the presence of a DC offset. As can be observed from Fig. 6(c), by the application of voltage, the transformer is driven into positive saturation, causing the actual flux to surpass λ^{max} and reach λ_{sat}. The positive saturation on *B-H* curves is shown in Fig. 7 as point 1.

At $t = t_1$, switches S_1 and S_4 are turned off while switches S_2 and S_3 are turned on. Due to the inductive nature of the transformer, the current does not change immediately and continues to flow through diodes D_2 and D_3 until it descends to zero at $t = t_2$. Throughout diode conduction (between t_1 and t_2), a negative voltage ($-V_{DC}$) is applied to the transformer, which accelerates the current reduction to zero. After $t = t_2$, the current continues to decrease, with switches S_2 and S_3 creating a path for the current. When switches S_2 and S_3 conduct, again $-V_{DC}$ is applied to the transformer. The current reduction continues until the measured current reaches $-0.1I_n$ at $t = t_3$, which is equivalent to $-\lambda_{sat}$ (i.e., negative saturation, marked as point 2 in Fig. 7). At $t = t_3$, switches S_2 and S_3 are turned off, and once more, switches S_1 and S_4 are turned on. The current flows through diodes D_1 and D_4 until it becomes zero at $t = t_4$, and then through switches S_1 and S_4 until it reaches $0.1I_n$ at $t = t_5$.

An important point to consider is that the voltage transducer's output usually contains a DC offset. This offset, if not dealt with properly, can make the flux estimation inaccurate. Let $v_p(t)$ show the voltage induced on the open-circuited primary winding. The voltage transducer adds the DC offset ΔV_{DC} to the signal, and outputs $v_p^m(t) = v_p(t) + \Delta V_{DC}$, where the superscript "m" is used to mark transducer measurements. To estimate the DC offset, $v_p^m(t)$ can be integrated from t_1 to t_5 and averaged as below

$$\Delta V_{DC} = \frac{1}{t_5 - t_1}\left[\int_0^{t_5} v_p^m(t)dt - \int_0^{t_1} v_p^m(t)dt\right] \quad (7)$$

where the integral of $v_p(t)$ over a full period ($t_5 - t_1 = T$) is zero. Now, let $i_{inj}(t)$ denote the current injected into the secondary winding and $i_{inj}^m(t) = i_{inj}(t) + \Delta I_{DC}$ where the variable on the left-hand side denotes the measured current and ΔI_{DC} expresses the DC offset in this measurement, respectively. The DC offset ΔI_{DC} can be determined from:

$$\Delta I_{DC} = \frac{1}{t_5 - t_1}\left[\int_0^{t_5} i_{inj}^m(t)dt - \int_0^{t_1} i_{inj}^m(t)dt\right] \quad (8)$$

Using (7) and (8), $v_p(t)$ and $i_{inj}(t)$ can be derived from the transducers' outputs. Now let us define the voltage integral $\lambda_v(t)$ as

$$\lambda_v(t) = \int_{t_5}^t v_p(t)\,dt \quad (9)$$

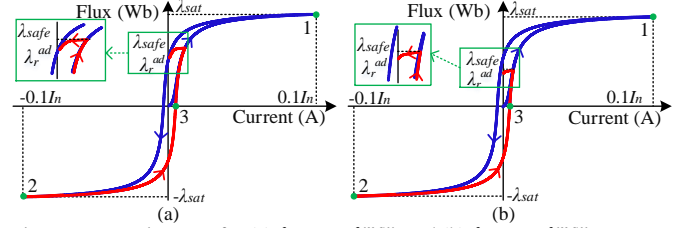By comparing Figs. 6(c) and 6(e), it can be seen that after

Fig. 7. Hysteresis curve for (a) $\lambda_{safe} > \lambda_r^{max}$, and (b) $\lambda_{safe} < \lambda_r^{max}$.

$t = t_5$, $\lambda_v(t)$ represents the actual flux which is shifted downward by $-\lambda_{sat}$, i.e., $\lambda_v(t) = \lambda(t) - \lambda_{sat}$. This allows us to estimate the actual flux by λ_v.

The transformer is subject to a negative voltage at $t = t_5$, leading to negative saturation at $t = t_7$. At this time, $\lambda_v(t_7)$ reaches $-2\lambda_{sat}$, as shown in Fig. 6(e). Therefore, one can readily obtain λ_{sat} from:

$$\lambda_{sat} = \frac{1}{2}(\lambda_v(t_5) - \lambda_v(t_7)) \quad (10)$$

After $t = t_7$, switches S_2 and S_3 are turned off, and a positive voltage is applied to the transformer firstly through diodes D_1 and D_4 and then through switches S_1 and S_4. The positive voltage changes the voltage integral λ_v from $-2\lambda_{sat}$ to $-\lambda_{sat}$ at $t = t_9$, corresponding to a rise from $-\lambda_{sat}$ to zero in actual flux (representing core demagnetization, marked as point 3 in Fig. 7). The voltage integral further increases to $-\lambda_{sat} + \lambda_{safe}$ at $t = t_{10}$, which corresponds to λ_{safe} in the actual flux, as shown in Fig. 6(c). Once $\lambda_v(t_{10})$ reaches $-\lambda_{sat} + \lambda_{safe}$, switches S_1 and S_4 are turned off, and current flows through diodes D_2 and D_3, applying negative voltage to the transformer. This voltage facilitates the process of current reduction to zero. At $t = t_{11}$, current reaches zero and remains unchanged since switches S_2 and S_3 are turned off. This current reduction causes the actual flux to reduce from λ_{safe} and reaches a value lower than λ_{safe} at $t = t_{11}$ due to the hysteresis phenomenon. This settling value of the adjusted residual flux can be obtained from

$$\lambda_r^{ad} = [\lambda_{sat} + \lambda_v(t_{11})] \quad (11)$$

Fig. 7 shows the hysteresis loops traversed during flux adjustment for two different scenarios. One scenario is where $\lambda_{safe} > \lambda_r^{max}$ and another is where $\lambda_{safe} < \lambda_r^{max}$. The actual flux's transition from $-\lambda_{sat}$ to λ_r^{ad} is highlighted in red. In the former case, the adjusted residual flux lies on the maximum feasible residual flux, as depicted in Fig. 7(a). In the latter scenario, the adjusted residual flux falls within the feasible range $[-\lambda_r^{max}, \lambda_r^{max}]$, as shown in Fig. 7(b). Both scenarios prevent making on the previous hump and reduce the impact of scatters on transformer energization.

C. Controlled Switching Stage

The next stage after flux adjustment is transformer energization. Without loss of generality, let us assume that the nominal voltage $v(t) = V_m cos(\omega t)$ is applied to the primary winding of the transformer while the secondary winding is open-circuited. The hat sign is used to refer to the per-unit flux with λ^{max} as the base value. The phase angle of the rising half of the gap voltage that results in a match between residual and
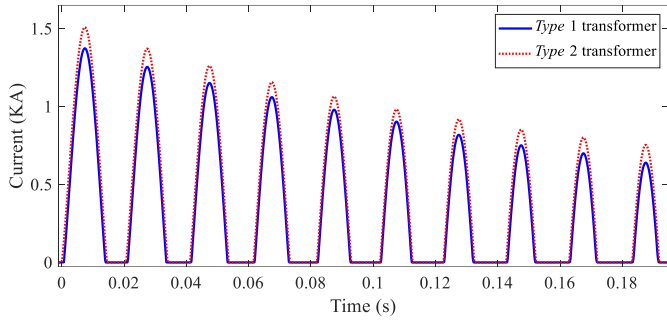
Fig. 8. Transformers' inrush currents in the worst-case energization scenarios.

TABLE I
DIFFERENT SCATTER'S IMPACT ON THE MPFM'S PERFORMANCE

RDDS		s^{min}	s^{mean}	s^{max}
Closing Time		$T_{CB} - \Delta T_{CB}$	T_{CB}	$T_{CB} + \Delta T_{CB}$
Type 1	t_{ct} (ms)	12.7	14.2	15.7
	t_m (ms)	6.8	8	9.7
	$\hat{\lambda}_r^{ad}$	0.84	0.6	0.09
Type 2	t_{ct} (ms)	11.8	13.3	14.8
	t_m (ms)	6.6	7.6	9.1
	$\hat{\lambda}_r^{ad}$	0.88	0.68	0.28

prospective fluxes is calculated from:

$$\varphi = \pi - \sin^{-1}(\hat{\lambda}_r^{ad}) \tag{12}$$

The making instant corresponding to φ is $t_m = \varphi/2\pi f$, where f is the power system frequency. The contact touch and closing operation initiation instants can be calculated from

$$t_{ct} = t_m + \frac{V_m cos(\omega t_m)}{s^{mean}} \tag{13}$$

$$t_{in} = t_{ct} - T_{CB} \tag{14}$$

The initiation of the closing operation of the CB at t_{in} guarantees that the prospective flux ideally matches the adjusted flux by making at t_m. Thanks to the considerations made to account for the impact of scatter in the closing operation of the CB, the difference between the two fluxes would be minimal.

V. PERFORMANCE EVALUATION

The results of simulation and experimental evaluation studies are presented and discussed in this section. A 25-MVA, 220 kV/27.5 kV core-type single-phase transformer is modeled using the terminal duality method (TDM) [36] in PSCAD/EMTDC. The nonlinear behavior of the core is simulated by the inverse Jiles-Atherton model [37-39]. Two different cores are studied with different hysteresis loops, referred to as Type 1 and Type 2, respectively. Both types exhibit a maximum flux density of ±1.5 T during normal operation. The ratio of the maximum residual flux to the maximum flux ($\lambda_r^{max}/\lambda^{max}$) for Type 1 and Type 2 cores is 0.6 and 0.75, respectively. The parameters of the inverse Jiles-Atherton model for both types can be found in [29]. The CB closing operation is modeled considering mechanical and RDDS scatter as random variables with normal distributions [33]. The pre-fluxing device shown in Fig. 5 is used for flux adjustment, with a DC-link voltage of 60 V. In addition, an HIL test system including a single-phase transformer and a pre-
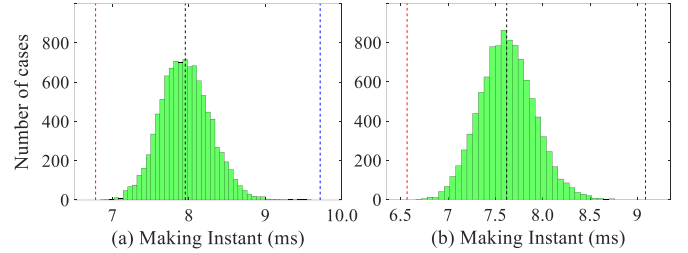

Fig. 9. (a) Type 1, and (b) Type 2 transformers' making instant distributions.

fluxing device is used to experimentally investigate the MPFM's performance.

The Type 1 and Type 2 transformers are first randomly energized to investigate the size of inrush current that can be drawn by each. Then, the proposed method is extensively tested in the presence of the uncertainties associated with the CB closing operation. The focus in Subsection V-C is on the flux adjustment process proposed in the paper. The MPFM, CPFM [28], demagnetization [25], and random energization methods are compared in Subsection V-D. Lastly, experimental validation results and findings are outlined and discussed.

A. Random Energization of Single-phase Transformer

Energizing a transformer without taking measures to limit inrush current is known as random energization. In this assessment, the closing operation is uniformly distributed over a 20 ms interval, and the residual flux is assumed to be any random value within the feasible range. The RDDS and closing time of the CB is assumed to vary in the ranges [28 kV/ms, 52 kV/ms], and [48.5 ms, 51.5 ms], respectively. The worst-case energization scenarios are those resulting in the maximum difference between the residual and prospective fluxes, thus the largest inrush current. These extreme cases are used as a reference to evaluate the distribution and magnitude of inrush current following random energization.

The currents that flow into the Type 1 and Type 2 transformers under these worst-case scenarios are shown in Fig. 8. As can be seen, the magnitude of inrush current drawn by the Type 1 and Type 2 transformers is as high as 1.37 kA and 1.5 kA, respectively. For each type, 1000 simulations are conducted to account for the random nature of variables. For the Type 1 transformer, the highest current magnitude ranges from 0.46 A to 1.37 kA with mean 739 A. For the Type 2 transformer, this lies in the range [0.32,1500] A with mean 788 A. As anticipated, the inrush current can exceed the nominal peak current (which is 160 A) by several times.

B. General Evaluation of the MPFM

To assess the performance of the MPFM, the same CB as the one used in the previous subsection is employed. The safe flux range, normalized by λ^{max}, expands from −0.7 pu to 0.7 pu. Following flux adjustment, the adjusted residual flux for Type 1 and Type 2 transformers, normalized with respect to λ^{max}, are 0.6 pu and 0.69 pu, respectively. A sensitivity analysis is carried out by conducting 10,000 simulations for each transformer, evaluating the impact of scatter values on the MPFM's performance. The outcomes of this analysis are presented in Table I. For Type 1 and Type 2 transformers, the making instants fall within the ranges of [6.8 ms, 9.7 ms] and
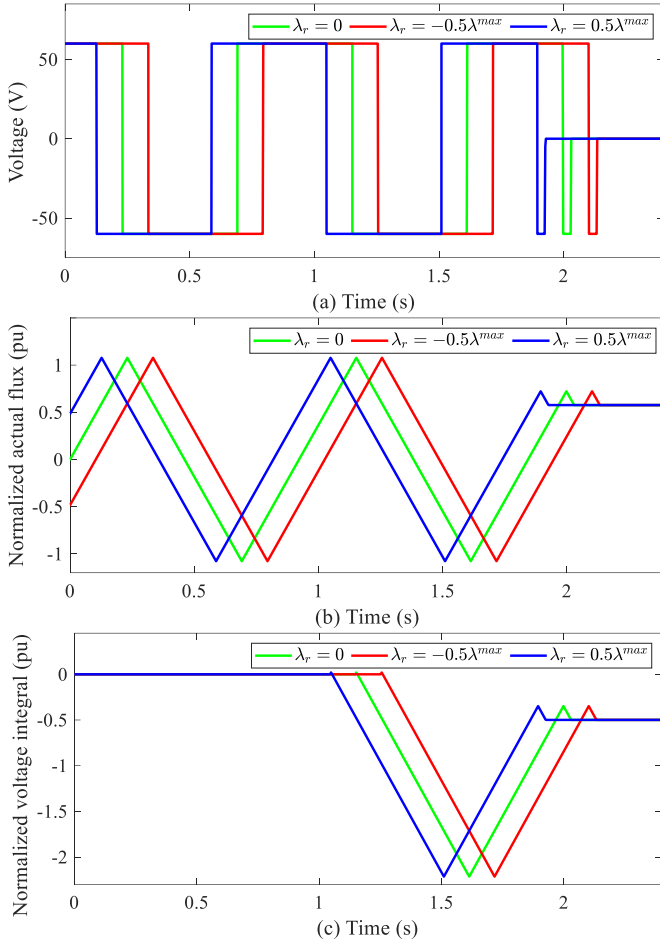
Fig. 10. (a) Voltage applied to the secondary winding, (b), normalized actual flux, and (c) normalized voltage integral.

[6.6 ms, 9.1 ms], respectively. Correspondingly, the values of $\hat{\lambda}_r^{ad}$ are [0.09 pu, 0.84 pu] and [0.28 pu, 0.88 pu].

The making instant distributions are demonstrated in Fig. 9. The probability of making occurrence is the highest at the ideal target making instants (8 ms and 7.6 ms for the two transformers) as marked by the dashed black lines. In most cases, there is only a slight difference between the true and ideal target making instants. The probability of making occurrence decreases as we go farther away from the ideal target making instant. This probability soon becomes zero at the upper and lower bounds of the making interval, indicated by the dashed blue and red lines. The impact of larger λ_r^{ad} is also shown in Fig. 9. A higher value of λ_r^{ad} results in a narrower making interval (as seen in the energization of the *Type* 2 transformer).

C. Flux Adjustment by the MPFM

The flux adjustment procedure for the *Type* 1 transformer is shown in Fig. 10. For this evaluation, the initial residual flux is set to zero, $-0.5\lambda^{max}$, and $0.5\lambda^{max}$, respectively. The DC offset on voltage and current transducer outputs is 100 V and 1 A. The safe flux range, normalized by λ^{max}, spans from -0.7 pu to 0.7 pu. The voltage applied to the secondary winding via the pre-fluxing device is shown in Fig. 10(a). As can be seen, the initial residual flux impacts the time required for flux adjustment by the MPFM. The fastest adjustment occurs when $\lambda_r = 0.5\lambda^{max}$, as the flux reaches λ_{sat} for the first
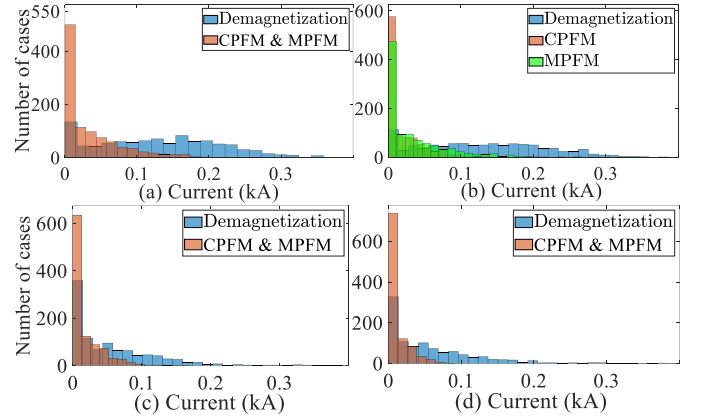

Fig. 11. (a) *Type* 1, slow CB, (b), *Type* 2, slow CB, (c) *Type* 1, fast CB, and (d) *Type* 2, fast CB.

TABLE II
FLUX ADJUSTMENT RESULTS

Type	λ_r/λ^{max}	-0.75	-0.50	-0.25	0	0.25	0.50	0.75
1	$\lambda_r^{ad}/\lambda^{max}$	N.A	0.60	0.60	0.60	0.60	0.60	N.A
	Eq. (11)	N.A	0.59	0.59	0.61	0.60	0.59	N.A
	t_{11}(s)	N.A	2.14	2.07	2.05	1.98	1.93	N.A
2	$\lambda_r^{ad}/\lambda^{max}$	0.69	0.69	0.69	0.69	0.69	0.69	0.69
	Eq. (11)	0.69	0.68	0.70	0.68	0.69	0.70	0.70
	t_{11}(s)	2.18	2.13	2.08	2.03	1.97	1.92	1.87

time more quickly. As λ_r decreases, the time needed for flux adjustment increases. Based on λ_r value, the MPFM needs 1.92 to 2.13 seconds for flux adjustment. The CPFM, however, requires nearly 10 minutes to flux this transformer.

In Fig. 10(b), the waveforms of actual flux normalized by λ^{max} are shown. Since the maximum feasible residual flux lies in the safe flux range, the residual flux is adjusted to the maximum feasible residual flux, i.e., $\lambda_r^{ad} = 0.6\lambda^{max}$. This figure also shows that regardless of the initial value of residual flux, the MPFM can easily adjust the residual flux to λ_r^{max}. Fig. 10(c) shows the voltage integral λ_v, normalized by λ^{max}. Substituting the voltage integral values at t_5, t_7, and t_{11} into equations (10) and (11), the per-unit value of adjusted residual flux is found to be 0.61, 0.59, and 0.59 for cases with $\lambda_r = 0$, $\lambda_r = -0.5\lambda^{max}$, and $\lambda_r = 0.5\lambda^{max}$, respectively. Table II summarizes the details of flux adjustment for both transformers, including the initial residual flux value, the true and estimated values of adjusted residual flux using (11), and the time taken for the flux adjustment. As shown, the MPFM adjusts the residual flux to a value within the safe flux range in a few seconds. The MPFM estimates the adjusted residual flux regardless of the initial residual flux value.

D. Comparison with Other Methods

This subsection compares MPFM with CPFM [28], demagnetization [25], and random energization methods. To assess the impact of CB closing operation on the methods' performance, two types of CBs are considered: A slow CB and a fast CB. For slow CB, $RDDS = 40$ kV/ms with $\pm 30\%$ scatter and $T_{CB} = 50$ ms, with a mechanical scatter of ± 1.5 ms. The fast CB has an $RDDS$ of 70 kV/ms with $\pm 15\%$ scatter and a closing time of 30 ms, with a mechanical scatter of ± 1.0 ms. The safe flux range, normalized by λ^{max}, for slow
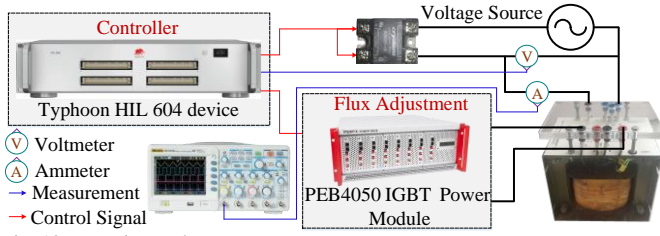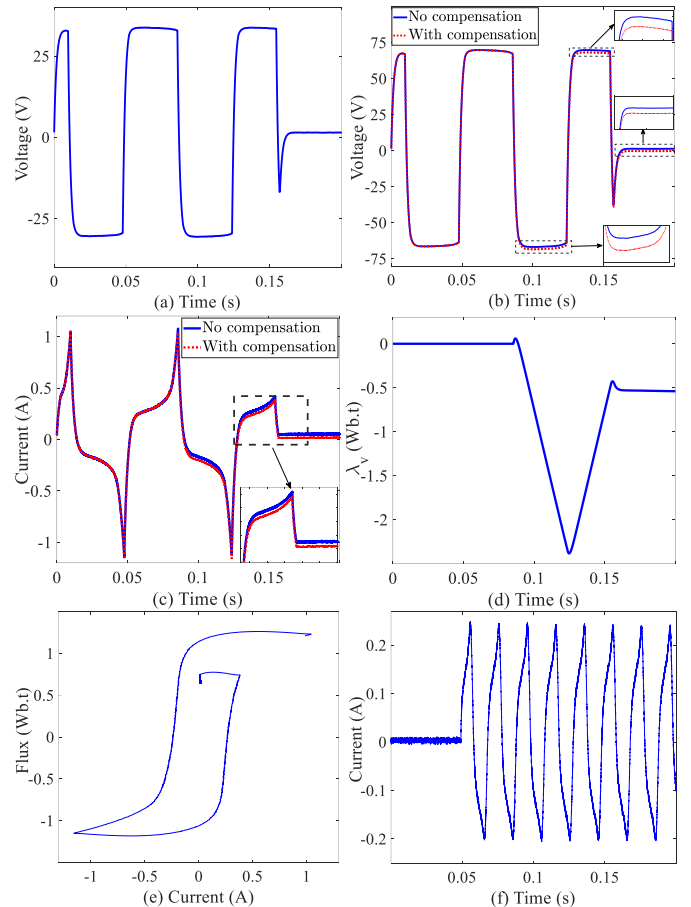
Fig. 12. Experimental setup.

Fig. 13. (a) Voltage applied to the secondary winding, (b), voltage induced on the primary winding, (c) secondary winding current, (d) voltage integral, (e) hysteresis curve after $t = 0.086$ s normalized by λ^{max}, and (f) primary winding current after transformer energization.

and fast CBs is $[-0.7\,\mathrm{pu}, 0.7\,\mathrm{pu}]$ and $[-0.96\,\mathrm{pu}, 0.96\,\mathrm{pu}]$, respectively. For each method, 4,000 simulations are conducted, using both CBs to energize the *Type* 1 and *Type* 2 transformers. The MPFM and CPFM adjust the residual flux to λ_r^{max}. However, for the case with the *Type* 2 transformer and slow CB, the MPFM adjusts the residual flux to $0.69\lambda^{max}$.

Fig. 11 shows the distributions of inrush current in numerous different conditions tested. Only results ranging from zero to 400 A are shown, and undesirable cases where making occurs on the previous hump using CPFM and demagnetization method are excluded. The MPFM is the only method that does not result in such undesirable makings. The results of random energization are excluded from Fig. 11 as they are uniformly spread out from zero to the highest attainable magnitude. As shown in Figs. 11(a), 11(c), and 11(d), both MPFM and CPFM exhibit a great performance. These two methods perform identically in all scenarios involving the *Type* 1 transformer and when a fast CB is used to energize the *Type* 2 transformer. In these cases, the peak current magnitude does not surpass 160 A, matching the peak amplitude of the nominal current. In the case of the *Type* 2 transformer with the slow CB, the CPFM demonstrates a superior performance in successful cases with MPFM ranking as the second-best method. Both methods limit the current well below the magnitude at the peak amplitude of the nominal current. However, CPFM suffers from making on the previous hump in about 1.0% of cases in which the current range from 600 A to 1100 A. The MPFM, however, remains unaffected, always limiting the current to 160 A.

E. Experimental Validation

A HIL test system shown in Fig. 12 is employed to experimentally examine the MPFM's performance. The system is composed of a 400-VA, 260 V/120 V shell-type single-phase transformer, a Typhoon HIL 604 device, a PEB4050 IGBT power module, and an HD6025-10 solid-state relay. The transformer's peak excitation current at the primary side is 0.22 A. This excitation current could reach 50 A in worst-case energization conditions. The HIL device controls the IGBT power module as the pre-fluxing device and the solid-state relay as a CB with associated *RDDS* and mechanical scatter. A 30-V DC voltage supplies the pre-fluxing device, and a 15-Ω resistor is included to cap the device's current at 2 A.

The MPFM's ability to adjust the residual flux to a value below $\hat{\lambda}_{safe} = 0.65$ pu is shown in Fig. 13. Figs. 13(a) and 13(b) demonstrate the voltage applied to the secondary winding and the induced voltage on the primary winding, respectively. At $t = 0.086$ s, the DC offset of the voltage transducer output is calculated, enabling the measurement of the actual voltage induced on the primary winding. Similarly, the DC offset compensation is implemented to the current transducer output, as seen in Fig. 13(c). Using the compensated voltage, the voltage integral $\lambda_v(t)$ is derived, as shown in Fig. 13(d). Equation (11) yields the value of the adjusted residual flux as 0.62 pu, also represented in Fig. 13(e) demonstrating the associated hysteresis loop after DC offset compensation. To validate the efficiency of the flux adjustment, the transformer is energized such that the prospective and residual fluxes are matched. The resulting current flowing into the transformer, energized by an ideal CB, is shown in Fig. 13(f). The current magnitude reaches 0.24 A, which closely matches the transformer excitation current. This proves the effectiveness of the MPFM in adjusting and estimating the residual flux.

VI. CONCLUSION AND FUTURE WORK

A modified pre-fluxing method (MPFM) is proposed in this paper to mitigate the inrush current of single-phase transformers. The concept of "safe flux range" is introduced and shown to play a vital role in flux matching-based methods. This range encompasses values that can be achieved as the residual flux of the core, as described, and can also be matched with the prospective flux, considering the operating characteristics and limitations of the circuit breaker (CB). A pre-fluxing device is developed for applying voltage to the

transformer and adjusting the residual flux to a suitable value within the safe flux range. Throughout the flux adjustment process, the MPFM compensates the DC offset of transducers, a critical step for estimating the residual flux and thus minimizing the difference between prospective and residual fluxes. The superiority of the MPFM over the conventional pre-fluxing method (CPFM) and demagnetization method is demonstrated through theoretical analysis, numerical simulations, and experimental testing.

In terms of reducing inrush current, both MPFM and CPFM demonstrate similar performances in most cases, effectively limiting the current magnitude to levels below the transformer's nominal current. This performance surpasses that of the demagnetization method significantly. The MPFM can quickly adjust the residual flux within a few seconds, even for high-power transformers. This is a great advantage while the CPFM requires several minutes to energize high-power transformers. The MPFM is designed in a way to account for and minimize the impact of uncertainties involved in CB closing operations. This proves necessary as the CPFM might occasionally suffer from making on the previous hump. Indeed, the MPFM retains all the benefits of the CPFM while removing its drawbacks. This paper only focuses on single-phase transformers; however, future work can extend the application of the MPFM to three-phase transformers.

REFERENCES

[1] T. Ortmeyer, "Three phase transformer banks," *Chapter 4, Electromechanical Machinery Theory and Performance*: IOP Publishing, 2018.

[2] W. S. Fonseca, *et al.*, "Analysis of structural behavior of transformer's winding under inrush current conditions," *IEEE Trans. Ind. Appl,* vol. 54, no. 3, pp. 2285-2294, 2018.

[3] Z. Lihua, *et al.*, "An improved magnetostriction model for electrical steel sheet based on Jiles–Atherton model," *IEEE Trans. Magn.,* vol. 56, no. 3, pp. 1-4, 2020.

[4] R. Hamilton, "Analysis of transformer inrush current and comparison of harmonic restraint methods in transformer protection," *IEEE Trans. Ind. Appl,* vol. 49, no. 4, pp. 1890-1899, 2013.

[5] A. Aktaibi, M. A. Rahman, and A. M. Razali, "An Experimental Implementation of the dq-Axis Wavelet Packet Transform Hybrid Technique for Three-Phase Power Transformer Protection," *IEEE Trans. Ind. Appl.,* vol. 50, no. 4, pp. 2919-2927, 2013.

[6] P. Mishra, A. Swain, A. K. Pradhan, and P. Bajpai, "Sequence Current based Inrush Detection in High Permeability Core Transformers," *IEEE Trans. Instrum Meas.,* vol. 72, pp. 1-9, 2023.

[7] A. Ameli, *et al.*, "Accurate fault diagnosis in transformers using an auxiliary current-compensation-based framework for differential relays," *IEEE Trans. Instrum Meas.,* vol. 70, pp. 1-14, 2021.

[8] M. Steurer, and K. Frohlich, "The impact of inrush currents on the mechanical stress of high voltage power transformer coils," *IEEE Trans. Power Del.,* vol. 17, no. 1, pp. 155-160, 2002.

[9] M. T. Hagh, and M. Valizadeh, "Analysis and comparative study of transient inrush current reduction methods," in 2007 Int. Conf. Power Eng. (IPEC 2007), 2007, pp. 287-291.

[10] Y. Cui, S. G. Abdulsalam, S. Chen, and W. Xu, "A sequential phase energization technique for transformer inrush current reduction-Part I: Simulation and experimental results," *IEEE Trans. Power Del.,* vol. 20, no. 2, pp. 943-949, 2005.

[11] H.-T. Tseng, and J.-F. Chen, "Voltage compensation-type inrush current limiter for reducing power transformer inrush current," *IET Electr. Power Appl.,* vol. 6, no. 2, pp. 101-110, 2012.

[12] M. M. Islam, K. M. Muttaqi, and D. Sutanto, "A saturated amorphous alloy core-based inrush current limiter to eliminate inrush currents and restrain harmonics during transformer energization," *IEEE Trans. Ind. Appl,* vol. 57, no. 6, pp. 6634-6645, 2021.

[13] T. Takamori, *et al.*, "Adjustable Current Limiting Function with a Monolithically Integrated SiC Circuit Breaker Device," *IEEE Trans. Ind. Appl.,* vol. 59, pp. 6427-6435, 2023.

[14] I. A. Pires, A. A. P. Machado, and B. de Jesus Cardoso Filho, "Mitigation of electric arc furnace transformer inrush current using soft-starter-based controlled energization," *IEEE Trans. Ind. Appl,* vol. 54, no. 4, pp. 3909-3918, 2018.

[15] S. J. Chapman, "Electric machinery fundamentals fifth edition," Mcgraw-hill, inc., 2012.

[16] Y. Wang, Z. Liu, and H. Chen, "Research on residual flux prediction of the transformer," *IEEE Trans. Magn.,* vol. 53, no. 6, pp. 1-4, 2017.

[17] R. Cano-González, A. Bachiller-Soler, J. A. Rosendo-Macías, and G. Álvarez-Cordero, "Controlled switching strategies for transformer inrush current reduction: A comparative study," *Electr. Power Syst. Res.,* vol. 145, pp. 12-18, 2017.

[18] J. Mitra, X. Xu, and M. Benidris, "Reduction of three-phase transformer inrush currents using controlled switching," *IEEE Trans. Ind. Appl,* vol. 56, no. 1, pp. 890-897, 2019.

[19] X. Lin, *et al.*, "Dynamic Dielectric Strength of C 3 F 7 CN/CO 2 and C 3 F 7 CN/N 2 Gas Mixtures in High Voltage Circuit Breakers," *IEEE Trans. Power Del.,* vol. 37, pp. 4032-4041, 2022.

[20] H. Zhang, *et al.*, "A New Method to Measure the Residual Flux by Magnetic Sensors and a Finite Element Model," *IEEE Trans. Instrum Meas.,* vol. 72, pp. 1-10, 2023.

[21] Y.-H. Chen, and P.-T. Cheng, "Flux estimation techniques for inrush current mitigation of line-interactive UPS systems," *IEEE Trans. Ind. Appl,* vol. 47, no. 2, pp. 901-911, 2011.

[22] C. a. o. WG, *Transformer energization in power systems: A study guide*, aris, France: CIGRE P, 2014.

[23] F. De Leon, *et al.*, "Elimination of residual flux in transformers by the application of an alternating polarity dc voltage source," *IEEE Trans. Power Del.,* vol. 30, no. 4, pp. 1727-1734, 2014.

[24] E. Hajipour, M. Salehizadeh, M. Vakilian, and M. Sanaye-Pasand, "Residual flux mitigation of protective current transformers used in an autoreclosing scheme," *IEEE Trans. on Power Del.,* vol. 31, no. 4, pp. 1636-1644, 2015.

[25] "Switchsync™ PWC600 Technical Manual," *Hitachi Energy* 2021.

[26] D. I. Taylor, J. D. Law, B. K. Johnson, and N. Fischer, "Single-phase transformer inrush current reduction using prefluxing," *IEEE Trans. Power Del.,* vol. 27, no. 1, pp. 245-252, 2011.

[27] D. I. Taylor, *System, apparatus, and method for reducing inrush current in a three-phase transformer*, to Google Patents, 2014.

[28] A. Aghazadeh, K. Li, V. Terzija, and S. Azizi, "Modified Pre-Fluxing Method for Energization of Single-Phase Transformers," in 2023 IEEE International Conference on Energy Technologies for Future Grids (ETFG), Wollongong, Australia, 2023, pp. 1-6.

[29] A. Aghazadeh, E. Hajipour, K. Li, and S. Azizi, "Mitigating the Inrush Current of V/V Transformers using Railway Conditioners," *IEEE Access,* vol. 12, pp. 50885-50897, 2024.

[30] C. A. Desoer, and E. S. Kuh, *Basic Circuit Theory*: Mcgraw-hill, inc., 1969.

[31] A. Kumar, R. Perveen, and U. Parikh, "Controlled switching of power transformer and shunt reactors for minimization of switching transients: a review," *Journal of The Institution of Engineers Series B*, pp. 1-12, 2021.

[32] S. Ghafourian, *et al.*, "General analysis of vacuum circuit breaker switching overvoltages in offshore wind farms," *IEEE Trans. Power Del.,* vol. 31, no. 5, pp. 2351-2359, 2016.

[33] H. Ito, *Switching Equipment*: Springer, 2019.

[34] U. Parikh, B. R. Bhalja, and E. Systems, "Challenges in field implementation of controlled energization for various equipment loads with circuit breakers considering diversified dielectric and mechanical characteristics," *Int j. electr. power energy syst.,* vol. 87, pp. 99-108, 2017.

[35] P. Bimbhra, *Electrical machinery*: Khanna Publishers, New Delhi, 2010.

[36] C. Álvarez-Mariño, F. De León, and X. M. López-Fernández, "Equivalent circuit for the leakage inductance of multiwinding transformers: Unification of terminal and duality models," *IEEE Trans. Power Del.,* vol. 27, no. 1, pp. 353-361, 2011.

[37] R. Naghizadeh, B. Vahidi, and S. Hosseinian, "Modelling of inrush current in transformers using inverse Jiles–Atherton hysteresis model with a neuro-shuffled frog-leaping algorithm approach," *IET Electr. Power Appl.,* vol. 6, no. 9, pp. 727-734, 2012.

[38] M. Popov, L. Van Der Sluis, G. Paap, and P. Schavemaker, "On a hysteresis model for transient analysis," *IEEE Power Engineering Review,* vol. 20, no. 5, pp. 53-55, 2000.

[39] M. Popov, L. Grcev, L. van der Sluis, and V. V. Terzija, "An ATP-EMTP-based model for analysis of shielding properties of ferromagnetic cable sheaths," *IEEE Trans. Power Del.,* vol. 20, no. 3, pp. 2241-2247, 2005.